Long-term Variations of CO_2 Trapped in Different Mechanisms in Deep Saline Formations: A Case Study of the Songliao Basin, China

Wei Zhang [1], Yilian Li [1], Tianfu Xu [2], Huilin Cheng [1], Yan Zheng [1], Peng Xiong [1]

[1] *School of Environmental studies, China University of Geosciences, Wuhan, 430074, China*

[2] *Earth Sciences Division, Lawrence Berkeley National Laboratory, University of California, Berkeley, CA 94720, USA*

Abstract The geological storage of CO_2 in deep saline formations is increasing seen as a viable strategy to reduce the release of greenhouse gases to the atmosphere. There are numerous sedimentary basins in China, in which a number of suitable CO_2 geologic reservoirs are potentially available. To identify the multi-phase processes, geochemical changes and mineral alteration, and CO_2 trapping mechanisms after CO_2 injection, reactive geochemical transport simulations using a simple 2D model were performed. Mineralogical composition and water chemistry from a deep saline formation of Songliao Basin were used. Results indicate that different storage forms of CO_2 vary with time. In the CO_2 injection period, a large amount of CO_2 remains as a free supercritical phase (gas trapping), and the amount dissolved in the formation water (solubility trapping) gradually increases. Later, gas trapping decreases, solubility trapping increases significantly due to migration and diffusion of the CO_2 plume, and the amount trapped by carbonate minerals increases gradually with time. The residual CO_2 gas keeps dissolving into groundwater and precipitating carbonate minerals. For the Songliao Basin sandstone, variations in the reaction rate and abundance of chlorite, and plagioclase composition affect significantly the estimates of mineral alteration and CO_2 storage in different trapping mechanisms. The effect of vertical permeability and residual gas saturation on the

overall storage is smaller compared to the geochemical factors. However, they can affect the spatial distribution of the injected CO_2 in the formations. The CO_2 mineral trapping capacity could be in the order of ten kilogram per cubic meter medium for the Songliao Basin sandstone, and may be higher depending on the composition of primary aluminosilicate minerals especially the content of Ca, Mg, and Fe.

***Keywords**:* Geological storage; Carbon dioxide; Numerical simulation; Saline formation; Songliao basin; China

1. Introduction

With the development of economies and an increase in human activities, global emissions of greenhouse gases (GHG) such as carbon dioxide (CO_2), methane (CH_4), nitrous oxide (NO_2) and chlorofluorocarbons (CFCs) have increased rapidly and lead to global climate change and ocean acidification with severe consequences for ecosystems and for human society (Holloway, 2001; West et al., 2005). CO_2 is responsible for about 64% of the greenhouse effect among the various greenhouse gases, and the average concentrations of CO_2 in the atmosphere have risen from a pre-industrial level (1750) of 280 parts per million by volume (ppmv) to over 370 ppmv currently and, if unabated, is projected to reach 1100 ppmv by 2100 (Bachu and Adams, 2003; Hepple and Benson, 2005; Kharaka et al., 2006). Thus, reducing the concentration of CO_2 in the atmosphere is very important to the mitigation of global climate change. The anthropogenic CO_2 emitted into the Earth's atmosphere originates mainly from the burning of fossil fuels to produce energy, which provide nowadays 75-85% of the world's energy demands (Holloway, 2001; Bachu and Adams, 2003; Allen et al., 2005). Even though increasing the efficiency of energy usage and/or developing lower carbon or non-carbon energies (e.g., natural gas, nuclear, wind, and biomass) to replace high carbon fuels (coal, oil) can reduce the accumulation of CO_2 in the atmosphere (Jean-Baptiste and Ducroux, 2003; Li et al., 2006), fossil fuels will still remain a major component of world's energy supply in the near future (Grimston et al., 2001) because of their inherent advantages, such as availability, competitive cost, ease of transport and storage, and large resources (Bachu, 2003; Bachu and Adams, 2003).

Therefore, other approaches have to be taken to reduce anthropogenic CO_2 emissions into the atmosphere. Currently, the research of CO_2 geological storage as a possible way is being extensively carried out. The main geologic formations include depleted or depleting oil and gas

reservoirs, un-mineable coal seams, and deep saline formations (Bachu et al., 1994; Hitchon et al., 1999). Injecting CO_2 into saline formations in sedimentary basins is one of the most promising methods of geological storage of CO_2 for the long-term sequestration of the gas. This is because saline formations are ubiquitous to sedimentary basins (Hitchon et al., 1999; Gunter et al., 2000), they have enough capacity to store large amounts of CO_2 from anthropogenic emissions, and there are shorter distances between most large CO_2 point sources and saline formations, which can minimize CO_2 transportation costs (Soong et al., 2004; Allen et al., 2005; Zerai et al., 2006). The injected CO_2 is stored by three trapping mechanisms in saline formations (Hitchon, 1996). First, CO_2 can be trapped as a gas or supercritical fluid in a formation, commonly called hydrodynamic trapping. Here we refer to this approach as "gas trapping". Second, CO_2 can dissolve into the groundwater, referred to as solubility trapping. The dissolution of CO_2 in groundwater increases the acidity of water and affects the dissolution of minerals composing the host rock matrix. Third, CO_2 can react directly or indirectly with minerals in the geologic formation leading to the precipitation of secondary carbonates. The latter process, so-called "mineral trapping", is potentially attractive because it could immobilize CO_2 for long-time scales, and prevent its easy return to the atmosphere.

The Energy Information Administration (EIA) of the U.S. Department of Energy (DOE) published the International Energy Outlook 2005 (IEO2005) which pointed out that China is the world's second largest emitter of CO_2 after the United States in 2002, accounting for 13.6% of the world's total CO_2 emissions (approximately 3.3 gigatons (Gt) of CO_2), and predicting that the CO_2 emissions in China will grow 4.0% per year, reaching 8.1 Gt CO_2 by 2025, and becoming the world's largest emitter of CO_2 (Meng et al., 2007). So the reduction of anthropogenic CO_2 emissions in China is very important and urgent.

Bai et al. (2006) estimated the total amount and distribution of CO_2 emitted from the major industrial point sources (e.g., power plants, cement production, steelworks, refineries, ethylene, ammonia, and ethylene oxide and hydrogen plants) in China. Their results indicated that the total emissions equals 2.96315×10^9 t CO_2, and these emissions are mainly concentrated in the eastern and central China. This is consistent with the population distribution and level of economic development in China. The studies of Zhou (2005) and Li et al. (2005) also indicated that there are numerous sedimentary basins in the eastern and central China, such as Songliao, Bohai Bay, Ordos, North Jiangsu and Sichuan basins located on land, and Yellow Sea, East China Sea, Pearl River Delta, Beibuwan and Yinggerhai basins located on the continental shelf (The total area is larger than 1.8×10^6 km^2). Large numbers of deep saline formations buried in the sedimentary basins are saturated with high concentration of dissolved solids, which make groundwater unsuitable to any large-scale exploitation. Friedmann (2003) pointed out that China's rich Mesozoic-Cenozoic tectonic and stratigraphic histories suggest a significant CO_2 storage potential (Meng et al., 2007). The extensive and concentrated distribution of CO_2 emission sources and sedimentary basins in the eastern and central China indicates that the development of CO_2 capture and storage (CCS) in China has a great potential.

Li et al. (2005) and Liu et al. (2005, 2006) estimated the CO_2 storage capacity in deep saline formations, coalbeds, and gas fields in China to be 1.43505×10^{11} t, 1.2078×10^{10} t, and 4.103×10^9 t, respectively. Yu et al. (2007) estimated that in China's coalbeds the CO_2 storage capacity is about 1.4267×10^{11} t. The main contributes of CO_2 sequestration in coalbed methane (CBM) zone are Qinghai, Eastern Ordos and Eastern Yunnan-Western Guizhou. Meng et al. (2007) estimated the economical availability of CO_2 storage demonstration projects in China. Although the above estimates and studies were not completely detailed and accurate, the

results still indicates that the development of CO_2 geological storage projects would be helpful for the reduction of anthropogenic CO_2 emissions in China.

In this paper, a reactive geochemical numerical simulation was used to model the CO_2 geological storage in a deep saline formation of Songliao Basin. The basin, located in northeastern China, is a large and productive basin covering an area of about 260,000 km^2 (Fig. 1). It is the most important oil-producing basin in China, accounting for one-third of the total national petroleum production. It is also one of the most important heavy industrial zones in China, having a large number of CO_2 emission sources such as power plants, cement production, steelworks, and oil and gas refiners. The research area used here is a sandstone formation of Xinli oilfield in central Songliao Basin.

This paper emphasizes the tremendous potential of CCS in China and aims to identify the long term trapping mechanisms in a deep saline formation of Songliao basin, which could be a suitable location for a CO_2 storage demonstration project. The objective of the study is to assess the multi-phase processes, geochemical changes and mineral alteration, and CO_2 trapping mechanisms over time up to 10,000 years when injecting 50 kg/s (corresponding to about 1.6 Mt of CO_2 per year) during 100 years, using coupled reactive-transport modelling. A sensitivity test is carried out to assess the influence on the unknown precise composition of the plagioclase mineral. Another sensitivity test is carried out on the kinetic rate of chlorite dissolution. The simulation results may be useful for the development of CO_2 demonstration projects in China.

2. Numerical approaches

2.1. Numerical tool

Simulations were performed using the non-isothermal multiphase reactive transport program TOUGHREACT (Xu and Pruess, 2001; Xu et al., 2006), which was developed by introducing reactive geochemical transport into the existing multiphase fluid and heat flow simulator TOUGH2 V2 (Pruess et al., 1999, 2004). The numerical method for solving fluid flow and chemical transport is based on an integral finite difference (IFD) method for space-discretization. The IFD method provides flexible discretization of geologic media by allowing the use of irregular grids, which is well suited for simulation of flow, transport, and fluid-rock interaction in heterogeneous and fracture rock systems with varying petrology. For regular grids, the IFD method is equivalent to the conventional finite difference method. An implicit time-weighting scheme is used for the flow, transport and kinetic geochemical equations. A sequential non-iterative approach is used for the coupling between transport and geochemical reactions. The program can be applied to one-, two-, or three-dimensional porous and fractured media with physical and chemical heterogeneity. It can accommodate any number of chemical species present in the liquid, gas and solid phases. A wide range of subsurface thermo-physical-chemical processes are considered under various thermohydrological and geochemical conditions such as pressure, temperature, ionic strength, pH and Eh.

2.2. Geological setting

The Songliao Basin is a large Mesozoic-Cenozoic intracratonic sedimentary basin developed

as the result of the initial rifting of the Eurasian Continent during the late Jurassic. It is bordered to the west by the Daxingan Mountains, to the north by the Xiaoxingan Mountains, to the east by the Zhangguangcai Mountains, and to the south by the Kangping-Kafu Hills; and the central area is a broad depression (Fig.1). This basin was formed first by rifting and then by subsidence and inversion. Based on the filling sequence and structures, the basin evolution can be divided into four phases (1) a pre-rift phase, (2) a syn-rift phase, (3) a post-rift phase, and (4) a compression phase (Hu et al., 1998; Zhou and Littke, 1999; Huang et al., 2004).

Fig. 2 shows the stratigraphy of the Songliao Basin (modified from Jin et al., 1999; Zhou and Littke, 1999; Huang et al., 2004). The stratigraphic sequence of non-marine deposits of upper Jurassic through Tertiary age is commonly divided into 10 Formations and more than 20 Members.

Xinli oilfield is located in Xinmiao town, Songyuan city, Jilin province of the northeastern China (Fig. 3). The sandstone formation, located in the third and fourth Members of the Lower Cretaceous Quantou Formation (K1q3 and K1q4), is a deep saline formation and oil producing unit, and the average thickness is about 50 m and the depth is around 1200 m. The location is considered as a potential candidate for CO_2 geological sequestration because it is close to the Changshan thermal and coal fired power plant (Fig. 3). In addition, CO_2 can be used to enhance oil recovery and store more CO_2. As Fig. 2 shown, the Lower Cretaceous Quantou Formation comprises interbedded shale, mudstone, and sandstone deposited in the lacustrine, delta environments (Cheng et al., 2006). The impermeable caprocks such as shale and mudstone are contributed to the safety of CO_2 geological storage.

2.3. Model setup

Much specific and detailed information is required to assess the feasibility of injection of CO_2 and to develop engineering designs for the injection systems. Before conducting site-specific investigations, general features and issues relating to the injected formation should be explored. This can be done by extracting the site-specific features and representing characteristics. Therefore, a simple two-dimensional (2D) radial model was used to study the temporal evolution and spatial distribution of the injected CO_2 and the subsequent geochemical changes. The 2D model was a homogeneous sandstone formation of 50 m thickness with a cylindrical geometrical configuration (Fig. 4). In the vertical direction, 10 model layers were used with a constant spacing of 5 m. In the horizontal direction, a radial distance of 100 km was modeled with a radial spacing that increases gradually away from the injection well. A total of 45 radial grid elements were used. The volume of the outer grid element is specified a large value of 10^{30} m^3, representing an infinitive lateral boundary. CO_2 injection was applied at the bottom portion of 10 m thickness with a constant rate of 50 kg/s (corresponding to 1.6 Mt/year) for a period of 100 years. The fluid flow and geochemical transport simulation was run for a period of 10,000 years.

2.4. Hydrogeochemical conditions

The hydrogeologic parameters used are listed in Table 1, the formation was assumed as homogenous. The petrophysical characteristics such as porosity and permeability were taken from the experimental measurements and data collection. The average porosity and permeability of the sandstone formation is 0.30 and 1.0×10^{-13} m^2, respectively. Due to the lack

of available data, other parameters such as those of the capillary pressure and relative permeability model were taken from Xu et al. (2006, 2007). A hydrostatic pressure distribution over the depth was specified initially.

The initial mineral composition of the sandstone formation used in the present simulations is derived from lithology slice analysis of the clastic rocks in the Songliao Basin (Table 2). It mainly consists of quartz, illite, chlorite, calcite, plagioclase and K-feldspar. Minor constituents include kaolinite, zeolite, pyrite and anhydrite. The composition of the plagioclase is uncertain, in which the ratio between albite and anorthite may affect the simulation results. Note that in other geochemical systems such as that of Gaus et al. (2005), anorthite did have an impact on the mineral trapping of CO_2. These investigators performed some kinetic batch modelling to assess the effects of different plagioclase compositions on the simulation results. Their results indicated that the CO_2 mineral trapping increases due to the presence of anorthite. However, in the modelling of Audigane et al (2007) all plagioclase is present as pure albite. Because albite is much more resistant to weathering than anorthite, Na will be the dominant cation in plagioclase. In our simulations we performed two simulations with different plagioclase compositions to assess their influence on the simulation results (see Section 3.2.2). In the first case all plagioclase is present as pure albite (base-case), in the second case oligoclase (containing both Na and Ca, see Table 2) is used to substitute plagioclase. The trace minerals zeolite, pyrite, and anhydrite are not included in the simulations. Magnesite, dolomite, siderite, ankerite, dawsonite, Na-smectite and Ca-smectite could be formed after CO_2 injection and are specified as secondary minerals in the simulations. Chalcedony is also included as a secondary silica phase, because at low temperature such as 50 ^{o}C considered in the present study, dissolved silica is thermodynamically controlled by chalcedony rather than quartz.

Halite may be formed close to the injection well because water evaporates into the injected CO_2 stream (André et al., 2007). The effect of formation of halite close to the well on the evaluation of the amounts and variations of long-term CO_2 trapped in different mechanisms is very small. Therefore, halite was not considered in the current simulation. Simulation results could be sensitive to the choice of secondary minerals. However, almost all possibilities of secondary carbonate and clay minerals are covered in the simulations, which are based on previous studies of modelling (Xu et al., 2005, 2006, 2007; Gaus et al., 2005; White et al., 2005), laboratory experiments (Wolf et al., 2004; Chen et al., 2006), and field observations (Pearce et al., 1996; Watson et al., 2004; Moore et al., 2005; Worden 2006).

The formation water is dominated by $NaHCO_3$ water type like the whole basin (Cheng et al., 2006). The concentration of total dissolved solids (TDS) ranges from 7,000 to 10,000 mg/L. Chloride is a very important anion in the area (the content exceeds 4,000 mg/L). Prior to simulating reactive transport, batch geochemical modeling of water-rock interaction was performed to generate an aqueous-phase chemical composition closely approaching the composition of a typical formation brine by equilibrating a 0.171 M (mol/kg H_2O) solution of sodium chloride in the presence of the primary minerals listed in Table 2 (with CO_2 gas pressure of 0.01 bar at a temperature of 50°C). A reasonably short simulation time (10 years in the present study) is needed to obtain a quasi-stable (or nearly steady-state) aqueous solution composition (Table 3). An initial pH of 8.343 was obtained, which is highly depends on CO_2 gas partial pressure used. If using a higher CO_2 pressure, the initial pH will be lower. We are primarily interested in the region affected by CO_2 injection. The uncertainty of background CO_2 pressure on simulation results should be very small for our objectives.

2.5. Kinetics of mineral dissolution and precipitation

A general kinetic rate law for mineral dissolution and precipitation is used (Lasaga et al., 1994; Steefel and Lasaga, 1994)

$$r_m = \pm k(T)_m A_m \left| 1 - \left(\frac{Q_m}{K_m} \right)^{\theta} \right|^{\eta} \quad (1)$$

where m is the kinetic mineral index, r_m is the dissolution/precipitation rate (positive values indicate dissolution, negative values indicate precipitation), $k(T)_m$ is the rate constant depending on the temperature (mol/m^2 s), T is the absolute temperature, A_m is the specific reactive surface area per kg water, K_m is the equilibrium constant for the mineral-water reaction written for the destruction of one mole of mineral m, and Q_m is the corresponding ion activity product. The parameters θ and η are two positive numbers determined by experiments; usually, but not always, they are taken to be equal to 1 (like in the present work).

For many minerals the kinetic rate constant $k(T)$ can be summed from three mechanisms (Lasaga et al., 1994; Palandri and Kharaka, 2004):

$$k(T) = k_{25}^{nu} \exp\left[\frac{-E_a^{nu}}{R} \left(\frac{1}{T} - \frac{1}{298.15} \right) \right] + k_{25}^{H} \exp\left[\frac{-E_a^{H}}{R} \left(\frac{1}{T} - \frac{1}{298.15} \right) \right] \alpha_H^{n_H} + k_{25}^{OH} \exp\left[\frac{-E_a^{OH}}{R} \left(\frac{1}{T} - \frac{1}{298.15} \right) \right] \alpha_{OH}^{n_{OH}} \quad (2)$$

where superscripts and subscripts *nu*, *H*, and *OH* indicate neutral, acid and base mechanisms, respectively, E_a is the activation energy, k_{25} is the rate constant at 25 °C, R is the gas constant (8.31 J/mol K), and T is the absolute temperature, α is the activity of the species, and n is a power term (constant). Notice that parameters θ and η (see Eq. (1)) are assumed to be the same for each mechanism. For all minerals it is assumed that the precipitation rate equals the dissolution rate.

Table 4 lists parameters for the kinetics of dissolution and precipitation of all minerals used in the simulations. Calcite is assumed to react with aqueous species at local equilibrium

because its reaction rate is typically quite rapid. The dissolution and precipitation of other minerals are kinetically controlled. Rate law parameters for kaolinite, illite, chlorite, albite-low, oligoclase, K-feldspar, magnesite, and dolomite were taken from Palandri and Kharaka (2004), who compiled and fitted experimental data reported by many investigators. The detailed list of the original data sources is given in Palandri and Kharaka (2004). Chalcedony kinetic data were referred to Tester (1994). Illite kinetic data were set to those of smectite. Siderite kinetic data were from Steefel (2001). Ankerite and dawsonite kinetic data were set to these of siderite. Xu et al. (2005) performed sensitivity simulations regarding ankerite and dawsonite precipitation kinetics, and results indicated that changes in the reaction rate result in small changes in their precipitation because the precipitation requires reactants whose availability is controlled by the slow dissolution of aluminosilicate minerals.

Mineral reactive-surface areas (the second column of Table 4) are based on the work of Sonnenthal et al. (2005), and were calculated assuming a cubic array of truncated spheres constituting the rock framework. The larger surface areas for clay minerals (kaolinite, illite and smectite) are due to smaller grain sizes. In conformity with White and Peterson (1990) and Zerai et al. (2006), a surface roughness factor of 10 is incorporated and defined as the ratio of the true (BET) surface area to the equivalent geometric surface area. Interaction with the minerals is generally expected to occur only at selective sites of the mineral surface, and the actual reactive surface area could be between one and three orders of magnitude less than the surface roughness-based surface area (Lasaga, 1995; Zerai et al. 2006). The difference is attributed to the fact that only part of the mineral surface is involved in the reaction due to coating or armoring, a small area exposed to the brine, and channeling of the reactive fluid flow. To account for these effects, the actual reactive surface areas given in Table 4 are decreased by

two orders of magnitude from the surface roughness-based surface areas. The reactive surface areas used here for most minerals are similar to those of Zerai et al. (2006), who used a surface area of 10 cm^2/g for all minerals.

If the aqueous phase supersaturates with respect to a potential secondary mineral, a small volume faction such as 1×10^{-6} is used for calculating the seed surface area for the new phase to grow. The precipitation of secondary minerals is represented using the same kinetic expression as that for dissolution. However, because precipitation rate data for most minerals are unavailable, parameters for neutral pH rates only, as given in Table 4, were employed to describe precipitation. Multiple kinetic mechanisms for precipitation can be specified in an input file of the TOUGHREACT program, should such information become available.

The evolution of the surface area in natural geologic media is very complex, especially for multi-mineral systems, and is not quantitatively understood at present. The magnitudes of surface areas specified are highly uncertain. We performed sensitivity simulations regarding the kinetic rate constants and/or reactive surface areas to partially address this issue. Details are given in Section 3.2.1.

3. Results and discussion

3.1. Base case

3.1.1. Gas and solubility trapping

The injected supercritical CO_2 fluid (called "gas" here for simplicity) at the bottom of the storage formation migrates upward rapidly by buoyancy forces because the density of supercritical CO_2 phase is lower than that of aqueous phase. A small fraction of CO_2 gas is trapped in the porous rock as residual gas after injection, and most of the free CO_2 gas

accumulates below the caprock.

The injected CO_2 is dissolved in the surrounding formation water, forming H_2CO_3 (aq), HCO_3^-, and CO_3^{2-}, and increasing acidity (Druckenmiller and Maroto-Valer, 2005; Rosenbauer et al., 2005):

$$CO_2(gas) \leftrightarrow CO_2(aq) \tag{3}$$

$$CO_2(aq) + H_2O \leftrightarrow H_2CO_3 \tag{4}$$

$$H_2CO_3 \leftrightarrow H^+ + HCO_3^- \tag{5}$$

$$HCO_3^- \leftrightarrow H^+ + CO_3^{2-} \tag{6}$$

Then, the increased acidity induces dissolution of many of the primary host rock minerals. The mineral dissolution increases concentrations of cations such as Na^+, Ca^{2+}, Mg^{2+}, and Fe^{2+}, which in turn causes complexing of dissolved cations with the bicarbonate ion to form $NaHCO_3$, $CaHCO_3^+$, $MgHCO_3^+$, and $FeHCO_3^+$, such as

$$Ca^{2+} + HCO_3^- \leftrightarrow CaHCO_3^+ \tag{7}$$

Over time they tend to increase CO_2 solubility and enhance solubility trapping.

In the upper portions of the reservoir, CO_2 dissolution into groundwater increases the density of the aqueous phase. Aqueous phase will then move downward due to gravity, giving rise to "convective mixing" (Ennis-King and Paterson, 2007). This CO_2 dissolution process and subsequent aqueous-phase convection will tend to mix aqueous CO_2 in the vertical direction. The density-driven convection will accelerate the dissolution of the free CO_2 gas.

Figs. 5 and 6 show the spatial distribution of CO_2 gas saturation and dissolved CO_2 concentration in the saline formation after different times. The CO_2 gas saturation in porous rock increases with the injection of CO_2 (Fig. 5), especially the area around the injection well. In about 100 m radial distance rock pores are completely filled by CO_2 gas at 100 years (complete water drying out zone). After injection ends (at 100 years), with the coming back of

groundwater the chemical reactions (dissolution and precipitation) between the dissolved CO_2 and minerals occurs again. The CO_2 gas stored in porous rock gives rise to tension that makes a very small amount of the CO_2 gas immobile and permanently trapped (the saturation of the remaining gas is referred to as residual gas saturation, S_{gr}). For large values of S_{gr}, more CO_2 can be trapped in the pore space, hampering the long-term migration of the CO_2 plume away from its injection site. The residual CO_2 gas continues to dissolve into groundwater and precipitate carbonate minerals, consequently leading to more injected CO_2 being stored in the geologic medium. The effect of residual gas saturation on long-term geological storage of CO_2 will be discussed in Section 3.2.3. With the migration of CO_2 gas, the concentration of dissolved CO_2 rapidly increases, larger than 1 mol/kg H_2O in the two-phase region (Fig. 6). The dissolved CO_2 tends to migrate downward after 1,000 years, but it is not significant, because precipitation of carbonate minerals partially consume the dissolved CO_2.

3.1.2. Mineral trapping

Fig. 7 shows the spatial distribution of cumulative CO_2 sequestered by precipitation of secondary carbonate minerals. The amount of CO_2 sequestered by carbonate minerals only increases gradually after 1,000 years (Fig. 7). The maximum mineral trapping capacity of CO_2 after 10,000 years could reach about 8 kg per one m^3 medium. The injected CO_2 is mainly immobilized by precipitation of ankerite ($CaMg_{0.3}Fe_{0.7}(CO_3)_2$) (Fig. 8). Precipitation of ankerite requires Ca^{2+} provided by the dissolution of calcite ($CaCO_3$) (Fig. 9), Mg^{2+} and Fe^{2+} provided by the dissolution of chlorite ($Mg_{2.5}Fe_{2.5}Al_2Si_3O_{10}(OH)_8$) (Fig. 10). The CO_2 mineral trapping capability depends on the dissolution of primary aluminosilicate minerals containing Ca, Mg, and Fe like chlorite in this case. In Section 3.2.2 we will discuss the effect of change in chlorite abundance on the simulation results. Note that dissolution of one mole of calcite ($CaCO_3$) leads precipitation of one mole of ankerite $CaMg_{0.3}Fe_{0.7}(CO_3)_2$, with more cations Mg^{2+} and Fe^{2+} in addition to Ca^{2+} and an extra mole of (CO_3) entity. Therefore, net balance is

CO_2 mineral trapping.

The increased concentration of H^+ in aqueous phase induced by CO_2 injection interacts with aluminosilicate and/or silicate minerals such as feldspars and clay minerals releasing cations such as Ca^{2+}, Mg^{2+}, and Fe^{2+}. The dissolved bicarbonate species reacts with these divalent cations to precipitate carbonate minerals, sequestrating CO_2 permanently. Lackner et al. (1995) found that the precipitation of carbonate minerals requires involvement of silicate rocks rich in Mg and Ca. Fyfe et al. (1996) also found that silicate minerals such as olivine could be sources of Ca and Mg (Hitchon et al., 1999; Gentzis, 2000; Cipolli et al., 2004). Therefore, siliciclastic (sandstone) formations are considered better candidates for CO_2 sequestration than carbonate formations which will partially dissolve due to low pH (Hitchon et al., 1999; Gentzis, 2000). This does not mean that carbonate formations are not suitable for the geological storage of CO_2, but that the dominant CO_2 trapping mechanisms in carbonate formations are solubility and gas trapping (Zerai et al., 2006).

3.1.3. Time evolution of the injected CO_2 in different trapping mechanisms

Amounts of CO_2 in different trapping mechanisms vary with time (Fig. 11). In the CO_2 injection period (0-100 years), a large amount of injected CO_2 remains as a free supercritical phase (gas trapping). The mass of CO_2 dissolved in the formation water gradually increases. After 100 years (injection end time), CO_2 gas trapping decreases, the amount of CO_2 dissolved in the formation water increases significantly because of the upward and horizontal migration of CO_2 plume and the convective mixing between CO_2-saturated water and unsaturated water. The amount of CO_2 trapped by precipitation of carbonate minerals increases gradually with time after 1,000 years.

3.2. Sensitivity analysis

Variations in mineral reaction rate and composition, and hydrological parameters may affect the simulation results, consequently the estimates of long-term CO_2 storage in different trapping mechanisms. In this Section, we examine uncertainties of simulation result to these factors.

3.2.1. Reaction rate

Xu et al. (2004, 2005) and Gaus et al. (2005) discussed the sensitivity of CO_2 mineral sequestration to kinetic rate constants or reactive surface areas. Their simulation results indicated that modifying the kinetic rate constants (or reactive surface areas) for all minerals by the same factor is equivalent to scaling the time-axis and does not lead to different results, and the key affecting the rate of the overall reactivity of the system is the kinetics of the dissolving aluminosilicate minerals bearing Ca, Mg, and Fe. As discussed above, chlorite containing Mg and Fe is a very important mineral. Here we examine the sensitivity of CO_2 mineral sequestration to dissolution kinetics of chlorite. Two additional simulations were carried out using respectively increasing and decreasing the reaction rate of chlorite by two orders of magnitude from the base case, Cases 2 and 3.

The increase of chlorite rate (Case 2) results in rapid dissolution of chlorite and calcite with time (Figs. 12 and 13). After 1,000 years chlorite dissolves completely (the initial volume fraction of chlorite is 0.027, see Table 2), which cannot provide more Fe^{2+} for precipitation of ankerite. The pattern of ankerite precipitation is similar to the base-case (Fig. 14), but the time and amount of the precipitation is different. The decrease of chlorite rate (Case 3) only causes

precipitation of some amount of siderite ($FeCO_3$) (Fig. 15). The precipitation of ankerite does not occur in this case, which is different from the base-case and Case 2. In the previous two cases, a very small amount of siderite precipitates only in the bottom of formation.

Fig. 16 shows the overall time evolution of the injected CO_2 in different trapping mechanisms for the three reaction rate cases. The total amount of CO_2 trapped in minerals increases with the increase of chlorite reaction rate (Case 2), while gas trapping decreases accordingly. Because CO_2 gas dissolution into brine is a very rapid process, the amount of CO_2 trapped in aqueous phase is relative stable. For Case 3 with the decrease of chlorite reaction rate, no significant CO_2 mineral trapping occurs. The results indicate that changes in the reaction rate of the dissolving aluminosilicate minerals containing Ca, Mg, and Fe like chlorite has a significant impact on mineral alteration and CO_2 storage in different mechanisms.

3.2.2. Mineral composition

Due to the uncertainty of mineral composition in actual geologic formations, two additional cases were performed to analyze the effect of variations in mineral composition: (1) an increase in chlorite abundance from 0.027 to 0.040 in volume fraction (Case 4), and (2) using oligoclase (bearing both Ca and Na) to substitute plagioclase (Case 5) instead of albite (bearing only Na) as used in the base-case.

Fig. 17 shows the time evolution of CO_2 stored in different trapping mechanisms for sensitivity simulations for different mineral composition. Increase in initial abundance of chlorite (Case 4) results in more dissolution of calcite and chlorite, and more precipitation of ankerite, consequently more CO_2 trapped in the solid phase, similar to those of Case 2 in Section 3.2.1. The amount of CO_2 trapped in gas phase decreases accordingly. The pattern of

the spatial distribution is similar to the base-case, so the results are not shown here.

Using oligoclase to substitute plagioclase (Case 5) obtained quite different results compared to the base-case (Fig. 17). The amount of CO_2 trapped in minerals is significantly increased especially after 1000 years, and gas trapping is significantly reduced accordingly. Solubility trapping is essentially unchanged. Injected CO_2 is immobilized by precipitation of dawsonite ($NaAlCO_3(OH)_2$), siderite and calcite, due to the dissolution of oligoclase ($Ca_{0.2}Na_{0.8}Al_{1.2}Si_{2.8}O_8$) and chlorite (Figs. 18 to 22). While in the base-case the precipitated carbonate mineral is essentially ankerite. Calcite precipitates in Case 5 instead of dissolution in the base-case because of supply of Ca^{2+} from dissolution of oligoclase. The maximum mineral trapping capacity of CO_2 after 10,000 years could reach about 55 kg per one m^3 medium (Fig. 23), which is significantly higher than that in the base-case.

3.2.3. Hydrological parameters

Hydrological parameters such as vertical permeability and residual gas saturation could have significant effects on simulation results (Lindeberg and Bergmo, 2002; Ennis-King et al., 2002; Kumar et al., 2004; Audigane et al., 2007). We performed two sensitivity simulations to examine these efforts. In Case 6, we reduced the ratio of vertical to horizontal permeability from 0.5 to 0.01 (Table 1). In Case 7, we increased the residual gas saturation from 0.05 to 0.20, corresponding to an efficient residual gas trapping (Audigane et al., 2007).

Decrease in vertical permeability (Case 6) results in significant decrease in the gas trapping, and increases in solubility and mineral trapping (Fig. 24). The lower value of vertical permeability in this case leads to a slower upward migration of injected CO_2 gas to the top of the formation, and a more rapid horizontal migration in middle and bottom of the formation,

resulting in more contact between injected CO_2 gas and formation waters and more dissolution of CO_2 gas (Fig. 25). For Case 7 with increase in residual gas saturation, amounts of CO_2 in different trapping mechanisms are slightly changed compared to the base-case during the CO_2 injection period (first 100 years). However, after injection stops, the gas trapping increases and the solubility trapping decreases. This is similar to the result of Audigane et al (2007). Increase in residual gas saturation limits CO_2 movement in the gas residing in porous rock (Fig. 26), which leads to decreasing contact between CO_2 gas and formation waters and decreasing dissolution of CO_2 gas.

The effect of the hydrological parameters on amounts of CO_2 storage in different trapping mechanisms is smaller than that of mineral reaction rate and abundance. However, variations in hydrological parameters can affect the spatial distribution of injected CO_2 in geologic formations, which is very important for studying the geological storage of CO_2.

4. Findings and conclusions

We have developed a 2D radial reactive transport model for the injection of CO_2 in a deep saline formation, using mineralogical composition and water chemistry encountered in Songliao Basin of China. Major findings and conclusions from simulations are summarized as follows:

1. Different storage forms of CO_2 vary with time. In the CO_2 injection period, a large amount of CO_2 remains as a free supercritical phase (gas trapping), and the amount dissolved in the formation water (solubility trapping) gradually increases. After injection stops, gas trapping decreases, solubility trapping increases slightly due to migration and diffusion of the CO_2 plume, and the amount trapped by precipitation of carbonate minerals increases

with time.

2. During the injection period, a small fraction of CO_2 gas is trapped in the porous rock as residual gas, and most of CO_2 gas accumulates below the caprock. Later, the CO_2 gas saturation decreases as it continues to disperse and further dissolve in groundwater. The bicarbonate in groundwater complexes with dissolved cations from aluminosilicate minerals further increases the solubility trapping. The residual gas keeps CO_2 dissolving into groundwater and precipitating carbonate minerals. As a result, the amount of CO_2 in the gas phase gradually decreases.
3. Limited numbers of sensitivity simulations have been performed. For the Songliao Basin sandstone, variations in the reaction rate and abundance of chlorite, and plagioclase composition affect significantly the estimates of mineral alteration and CO_2 storage in different trapping mechanisms. The effect of vertical permeability and residual gas saturation on the overall storage is smaller compared to the geochemical factors. However, they can affect the spatial distribution of the injected CO_2 in the formations.
4. The CO_2 mineral trapping capacity could be in the order of ten kilogram per cubic meter medium for Songliao Basin sandstone, and may be higher depending on the composition of primary aluminosilicate minerals especially the content of Ca, Mg, and Fe. In the base-case, precipitation of ankerite requires Ca^{2+} provided by the dissolution of calcite, Mg^{2+} and Fe^{2+} provided by the dissolution of chlorite. Variation in Ca content in Plagioclase affect significantly carbonate mineral precipitation, then amounts of CO_2 mineral trapping.

Because of rather significant reactivity of the storage reservoir, the potential impact on porosity and feedback on fluid flow and mechanical stability should be investigated in the

future. The range of problems concerning water-rock-CO_2 interaction is very broad. The present simulation results and conclusions are specific to the conditions and parameters considered. Due to computational constraints, our studies did not consider medium heterogeneities and geometric complexities. The "numerical experiments" presented here give a detailed view of the dynamical interplay between coupled hydrologic and chemical processes, albeit in an approximate fashion. A critical evaluation of modeling results can provide useful insight into the long-term CO_2 storage and geochemical performance.

Acknowledgements

The authors would like to thank Stefan Bachu and two anonymous reviewers for their constructive comments and suggestions during the review process, which greatly improve the quality of the paper. We would also like to acknowledge helpful comments from and discussions with colleagues Chenxi Wu, Liqun Sun and Sylvester Mumba. This work was supported by National Natural Science Foundation of China (NSFC, No. 40472122 and 40672168). The third author of this paper (Tianfu Xu) was supported by the Zero Emission Research and Technology project (ZERT) of the U.S. Department of Energy under Contract No. DE-AC02-05CH11231 with Lawrence Berkeley National Laboratory.

References

Allen, D.E., Strazisar, B.R., Soong, Y., Hedges, S.W., 2005. Modeling carbon dioxide sequestration in saline aquifers: Significance of elevated pressures and salinities. Fuel Process. Technol. 86, 1569-1580.

André, L., Audigane, P., Azaroual, M., Menjoz, A., 2007. Numerical modeling of fluid-rock chemical interactions at the supercritical CO_2-liquid interface during CO_2 injection into a carbonate reservoir, the Dogger aquifer

(Paris Basin, France). Energy Convers. Manage. 48, 1782-1797.

Audigane, P., Gaus, I., Czernichowski-Lauriol, I., Pruess, K., Xu, T., 2007. Two-dimensional reactive transport modeling of CO_2 injection in a saline aquifer at the Sleipner site, North Sea. Am. J. Sci. 307, 974-1008.

Bachu, S., Gunter, W.D., Perkins, E.P., 1994. Aquifer disposal of CO_2: hydrodynamic and mineral trapping. Energy Convers. Manage. 35, 269-279.

Bachu, S., 2003. Screening and ranking of sedimentary basins for sequestration of CO_2 in geological media in response to climate change. Environ. Geol. 44, 277-289.

Bachu, S., Adams, J.J., 2003. Sequestration of CO_2 in geological media in response to climate change: capacity of deep saline aquifers to sequester CO_2 in solution. Energy Convers. Manage. 44, 3151-3175.

Bai, B., Li, X.C., Liu, Y.F., Zhang, Y., 2006. Preliminary study on CO_2 industrial point sources and their distribution in China. Chinese J. Rock Mech. Eng. 25, 2918-2923. (in Chinese)

Chen, Z., O'Connor, W.K., Gerdemann, S.J., 2006. Carbonation for carbon sequestration and explanation of experimental results. Environ. Prog. 25, 161-166.

Cheng, J.M., McIntosh, J.C., Xie, X.N., Jiao, J.J., 2006. Hydrochemistry of formation water with implication to diagenetic reactions in Sanzhao depression and Qijia-gulong depression of Songliao Basin, China. J. Geochem. Explor. 88, 86-90.

Cipolli, F., Gambardella, B., Marini, L., Ottonello, G., Zuccolini, M.V., 2004. Geochemistry of high-pH waters from serpentinites of the Gruppo di Voltri (Genova, Italy) and reaction path modeling of CO_2 sequestration in serpentinites aquifers. Appl. Geochem. 19, 787-802.

Druckenmiller, M.L., Maroto-Valer, M.M., 2005. Carbon sequestration using brine of adjusted pH to form mineral carbonates. Fuel Process. Technol. 86, 1599-1614.

Ennis-King, J., Gibson-Poole, C.M., Lang, S.C., Paterson, L., 2002. Long-term numerical simulation of geological storage of CO_2 in the Petrel sub-basin, North West Australia, in APRC /GEODISC Project: Paper

http://www.apcrc.com.au/GEODISC%20PDFs/Ennis-King%20Long%20Term%20Simulation%20paper.pdf, 6 p.

Ennis-King, J., Paterson, L., 2007. Coupling of geochemical reactions and convective mixing in the long-term geological storage of carbon dioxide. Int. J. Greenhouse gas control 1, 86-93.

Gaus, I., Azaroual, M., Czernichowski-Lauriol, I., 2005. Reactive transport modeling of the impact of CO_2 injection on the clayey cap rock at Sleipner (North Sea). Chem. Geol. 217, 319-337.

Gentzis, T., 2000. Subsurface sequestration of carbon dioxide-an overview from an Alberta Canada perspective. Int. J. Coal Geol. 43, 287-305.

Grimston, M.C., Karakoussis, V., Fouquet, R., Van der Vorst, R., Pearson, P., Leach, M., 2001. The European and global potential of carbon dioxide sequestration in tacking climate change. Climate Policy 1, 155-171.

Gunter, W.D., Perkins, E.H., Hutcheon, I., 2000. Aquifer disposal of acid gases: modeling of water-rock reactions for trapping of acid wastes. Appl. Geochem. 15, 1085-1095.

Hepple, R.P., Benson, S.M., 2005. Geological storage of carbon dioxide as a climate change mitigation strategy: performance requirements and the implications of surface seepage. Environ. Geol. 47, 576-585.

Hitchon, B., 1996. Aquifer disposal of carbon dioxide. In: Hitchon, B. (ed.), Sherwood Park, Alberta, Canada: Geoscience Publishing Limited.

Hitchon, B., Gunter, W.D., Gentzis, T., Bailey, R.T., 1999. Sedimentary basins and greenhouse gases: a serendipitous association. Energy Convers. Manage. 40, 825-843.

Holloway, S., 2001. Storage of fossil fuel-derived carbon dioxide beneath the surface of the Earth. Annu. Rev. Energy Environ. 26, 145-166.

Hu, W.S., Cai, C.F., Wu, Z.Y., Li, J.M., 1998. Structural style and its relation to hydrocarbon exploration in the Songliao basin, northeast China. Mar. Petrol. Geol. 15, 41-55.

Huang, H.P., Yang, J., Yang, Y.F., Du, X.J., 2004. Geochemistry of natural gases in deep strata of the Songliao

Basin, NE China. Int. J. Coal Geol. 58, 231-244.

Jean-Baptiste, P., Ducroux, R., 2003. Energy policy and climate change. Energy Policy 31, 155-166.

Jin, Q., Xiong S.S., Lu, P.P., 1999. Catalysis and hydrogenation: volcanic activity and hydrocarbon generation in rift basins, eastern China. Appl. Geochem. 14, 547-558.

Kharaka, Y.K., Cole, D.R., Hovorka, S.D., Gunter, W.D., Knauss, K.G., Freifeld, B.M., 2006. Gas-water-rock interactions in Frio Formation following CO_2 injection: Implications for the storage of greenhouse gases in sedimentary basins. Geology 34, 577-580.

Kumar, A., Noh, M., Pope, G.A., Sepehrnoori, K., Bryant, S., Lake, L.W., 2004. Reservoir simulation of CO_2 storage in deep saline aquifers: Tulsa, Oklahoma, USA, 17-21 April 2004, Proceedings presented at the SPE/DOE 14th Symposium on Improved Oil Recovery, Paper SPE-89343.

Lasaga, A.C., Soler, J.M., Ganor, J., Burch, T.E., Nagy, K.L., 1994. Chemical weathering rate laws and global geochemical cycles. Geochim. Cosmochim. Ac. 58, 2361-2386.

Lasaga, A.C., 1995. Fundamental approaches in describing mineral dissolution and precipitation rates. In: White, A.F., Brantley, S.L. (Eds.), Chemical Weathering Rates of Silicates Minerals, Reviews in Mineralogy, vol. 31. BookCrafters, Chelsea, MI, pp. 23–86.

Li, X.C., Liu, Y.F., Bai, B., Fang, Z.M., 2005. Ranking and screening of CO_2 saline aquifer storage zones in China. Chinese J. Rock Mech. Eng. 25, 963-968. (in Chinese)

Li, Z., Dong, M., Li, S., Huang, S., 2006. CO_2 sequestration in depleted oil and gas reservoirs-caprock characterization and storage capacity. Energy Convers. Manage. 47, 1372-1382.

Lindeberg, E., Bergmo, P., 2002. The long term fate of CO_2 injected into an aquifer in Gale, J., and Kaya, Y., editors: Kyoto, Japan, 1-4 October 2002, Proceedings of the 6th International Conference on Greenhouse Gas Control Technology, p. 489.

Liu, Y.F., Li, X.C., Bai, B., 2005. Preliminary estimation of CO_2 storage capacity of coalbeds in China. Chinese J.

Rock Mech. Eng. 24, 2947-2952. (in Chinese)

Liu, Y.F., Li, X.C., Fang, Z.M., Bai, B., 2006. Preliminary estimation of CO_2 storage capacity in gas fields in China. Rock Soil Mech. 27, 2277-2281. (in Chinese)

Meng, K.C., Williams, R.H., Celia, M.A., 2007. Opportunities for low-cost CO_2 storage demonstration projects in China. Energy Policy 35, 2368-2378.

Moore, J., Adams, M., Allis, R., Lutz, S., Rauzi, S., 2005. Mineralogical and geochemical consequences of the long-term presence of CO_2 in natural reservoirs: An example from the Springerville-St. Johns Field, Arizona, and New Mexico, U.S.A. Chem. Geol. 217, 365-385.

Palandri, J.L., Kharaka, Y.K., 2004. A compilation of rate parameters of water-mineral interaction kinetics for application to geochemical modeling. US Geol Surv Open File Report 2004-1068, pp. 64.

Pearce, J.M., Holloway, S., Wacker, H., Nelis, M.K., Rochelle, C., Bateman, K., 1996. Natural occurrences as analogues for the geological disposal of carbon dioxide. Energy Convers. Manage. 37, 1123-1128.

Pruess, K., Oldenburg, C., Moridis, G., 1999. TOUGH2 user's guide, Version 2.0. Lawrence Berkeley Laboratory Report LBL-43134, Berkeley, California, USA.

Pruess, K., García, J., Kovscek, T., Oldenburg, C., Rutqvist, J., Steefel, C., Xu, T., 2004. Code intercomparison builds confidence in numerical simulation models for geologic disposal of CO_2. Energy 29, 1431-1444.

Rosenbauer, R.J., Koksalan, T., Palandri, J.L., 2005. Experimental investigation of CO_2-brine-rock interactions at elevated temperature and pressure: Implications for CO_2 sequestration in deep-saline aquifers. Fuel Process. Technol. 86, 1581-1597.

Sonnenthal, E., Ito, A., Spycher, N., Yui, M., Apps, J., Sugita, Y., Conrad, M., Kawakami, S., 2005. Approaches to modeling coupled thermal, hydrological, and chemical processes in the Drift Scale Heater Test at Yucca Mountain. Int. J. Rock Mech. Min. Sci. 42, 6987-719.

Soong, Y., Goodman, A.L., McCarthy-Jones, J.R., Baltrus, J.P., 2004. Experimental and simulation studies on

mineral trapping of CO_2 with brine. Energy Convers. Manage. 45, 1845-1859.

Steefel, C.I., Lasaga, A.C., 1994. A coupled model for transport of multiple chemical species and kinetic precipitation/dissolution reactions with applications to reactive flow in single phase hydrothermal system. Am. J. Sci. 294, 529-592.

Steefel, C.I., 2001. CRUNCH. Lawrence Livermore National Laboratory.

Tester, J.W., Worley, G.W., Robinson, B.A., Grigsby, C.O., Feerer, J.L., 1994. Correlating quartz dissolution kinetics in pure water from 25°C to 625 °C. Geochim. Cosmochim. Ac. 58, 2407-2420.

Watson, M.N., Zwingmann, N., Lemon, N.M., 2004. The Ladbroke Grove-Katnook carbon dioxide natural laboratory: A recent CO_2 accumulation in a lithic sandstone reservoir. Energy 29, 1457-1466.

West, J.M., Pearce, J., Bentham, M., Maul, P., 2005. Issue profile: Environmental issues and the geological storage of CO_2. Eur. Env. 15, 250-259.

White, A.F., Peterson, M.L., 1990. Role of reactive surface area characterization in geochemical models. Chemical modeling of aqueous systems II. In: Melchior, D.C., Bassett, R.L. (Eds.). Am. Chem. Soc. Symp. Ser. 416, 416-475.

White, S.P., Allis, R.G., Moore, J., Chidsey, T., Morgan, C., Cwynn, W., Adams, M., 2005. Simulation of reactive transport of injected CO_2 on the Colorado Plateau, Utah, USA. Chem. Geol. 217, 387-405.

Wolf, G.H., Chizmeshya, A.V.G., Diefenbacher, J., Mckelvy, M.J., 2004. In situ observation of CO_2 sequestration reactions using a novel microreaction system. Environ. Sci. Technol. 38, 932-936.

Worden, R.H., 2006. Dawsonite cement in the Triassic Lam Formation, Shabwa Basin, Yemen: A natural analogue for a potential mineral product of subsurface CO_2 storage for greenhouse gas reduction. Mar. Petrol Geol. 23, 61-77.

Xu, T., Apps, J.A., Pruess, K., 2005. Mineral sequestration of carbon dioxide in a sandstone-shale system. Chem. Geol. 217, 295-318.

Xu, T., Pruess, K., 2001. Modeling multiphase non-isothermal fluid flow and reactive geochemical transport in variably saturated fractured rocks: 1. Methodology. Am. J. Sci. 301, 16-33.

Xu., T, Apps, J.A., Pruess, K., 2004. Numerical simulation of CO_2 disposal by mineral trapping in deep aquifers. Appl. Geochem. 19, 917-936.

Xu, T., Sonnenthal, E., Spycher, N., Pruess, K., 2006. TOUGHREACT-A simulation program for non-isothermal multiphase reactive geochemical transport in variably saturated geologic media: Applications to geothermal injectivity and CO_2 geological sequestration. Comput. Geosci. 32, 145-165.

Xu, T., Apps, J.A., Pruess, K., Yamamoto, H., 2007. Numerical modeling of injection and mineral trapping of CO_2 with H_2S and SO_2 in a sandstone formation. Chem. Geol. 242, 319-346.

Yu, H.G., Zhou, G.Z., Fan, W.T., Ye, J.P., 2007. Predicted CO_2 enhanced coalbed methane recovery and CO_2 sequestration in China. Int. J. Coal Geol. 71, 345-357.

Zerai, B., Saylor, B.Z., Matisoff, G., 2006. Computer simulation of CO_2 trapped through mineral precipitation in the Rose Run Sandstone, Ohio. Appl. Geochem. 21, 223-240.

Zhou, D., 2005. Geological storage of CO_2-the new subject in geology. Prog. Nat. Sci. 15, 782-787. (in Chinese)

Zhou, Y.S., Littke, R., 1999. Numerical simulation of the thermal maturation, oil generation and migration in the Songliao Basin, Northeastern China. Mar. Petrol Geol. 16, 771-792.

Lists of Figures in the paper

Fig. 1

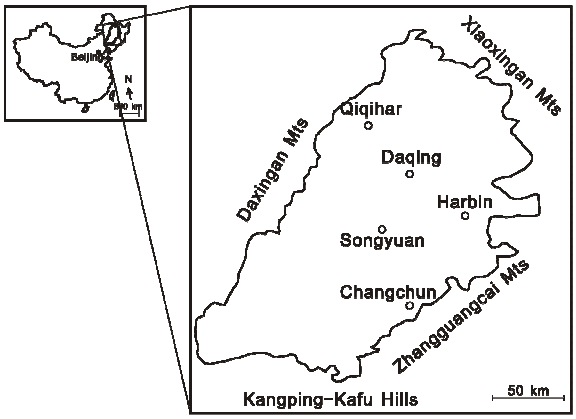
Beijing
N
800 km
Xiaoxingan Mts
Qiqihar
Daqing
Daxingan Mts
Harbin
Songyuan
Changchun
Zhangguangcai Mts
Kangping-Kafu Hills
50 km

Fig. 2

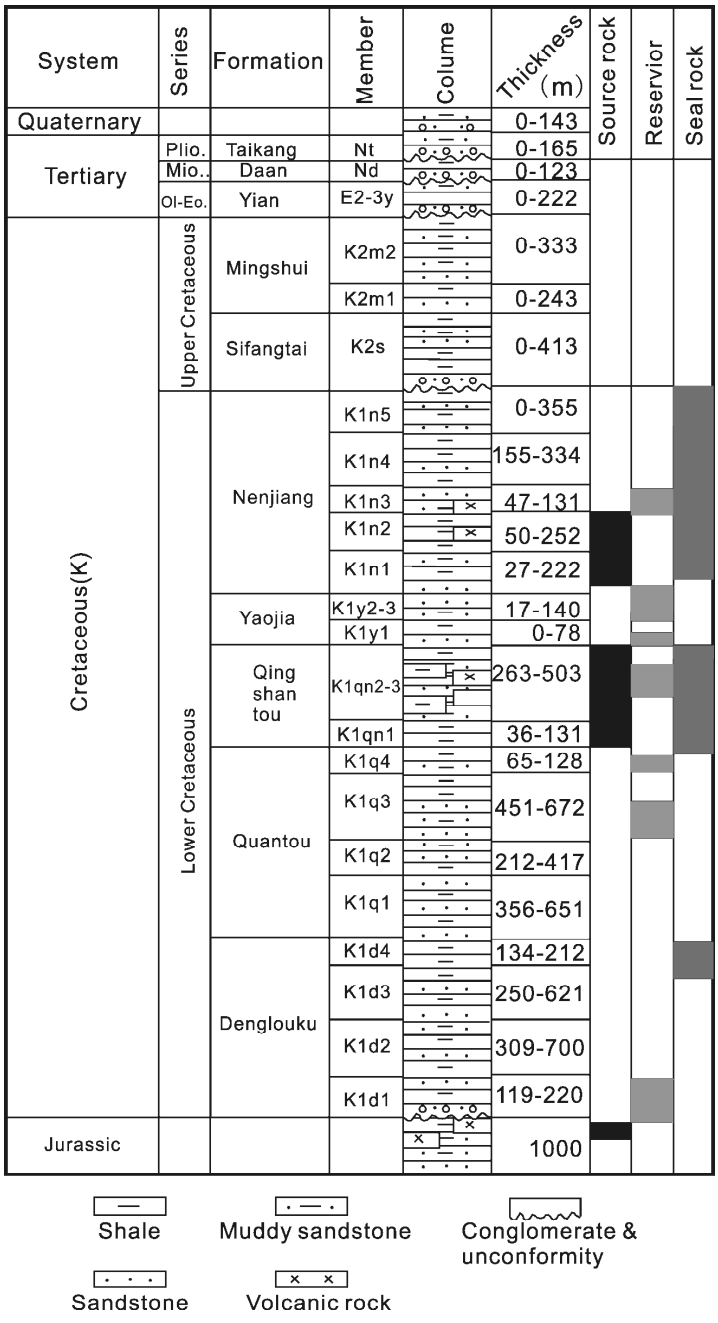
System
Series
Formation
Member
Colume
Thickness (m)
Source rock
Reservior
Seal rock
Quaternary
0-143
Tertiary
Plio.
Taikang
Nt
0-165
Mio.
Daan
Nd
0-123
Ol-Eo.
Yian
E2-3y
0-222
Cretaceous(K)
Upper Cretaceous
Mingshui
K2m2
0-333
K2m1
0-243
Sifangtai
K2s
0-413
Lower Cretaceous
Nenjiang
K1n5
0-355
K1n4
155-334
K1n3
47-131
K1n2
50-252
K1n1
27-222
Yaojia
K1y2-3
17-140
K1y1
0-78
Qing shan tou
K1qn2-3
263-503
K1qn1
36-131
Quantou
K1q4
65-128
K1q3
451-672
K1q2
212-417
K1q1
356-651
Denglouku
K1d4
134-212
K1d3
250-621
K1d2
309-700
K1d1
119-220
Jurassic
1000
Shale
Muddy sandstone
Conglomerate & unconformity
Sandstone
Volcanic rock

Fig. 3

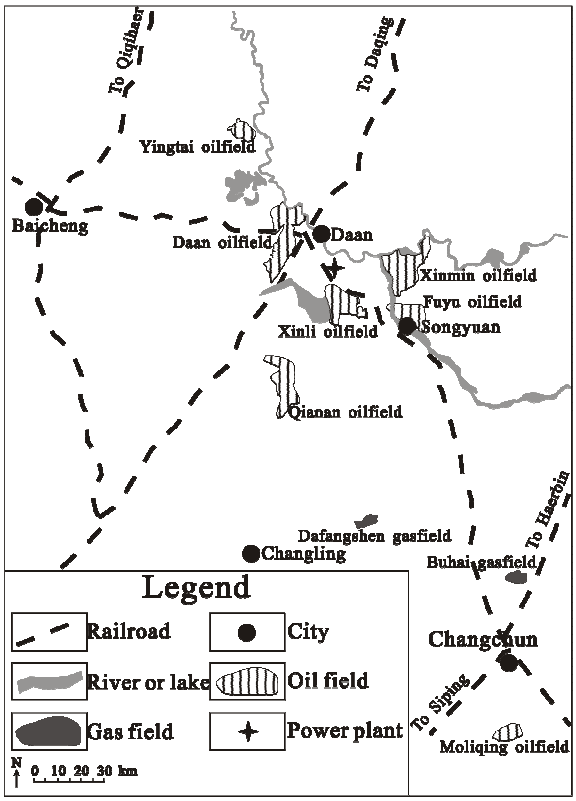
To Qiqihar
To Daqing
Yingtai oilfield
Baicheng
Daan oilfield
Daan
Xinmin oilfield
Fuyu oilfield
Songyuan
Xinli oilfield
Qianan oilfield
To Harbin
Dafangshen gasfield
Changling
Buhai gasfield
Changchun
To Siping
Moliqing oilfield
Legend
Railroad
City
River or lake
Oil field
Gas field
Power plant
N
0 10 20 30 km

Fig. 4

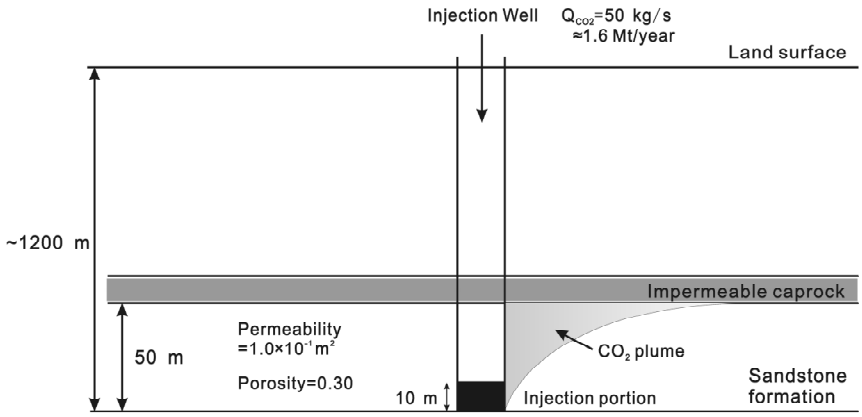
Injection Well
Q_{co2}=50 kg/s
≈1.6 Mt/year
Land surface
~1200 m
Impermeable caprock
50 m
Permeability
=1.0×10^{-1}m^2
Porosity=0.30
CO_2 plume
10 m
Injection portion
Sandstone
formation

Fig. 5

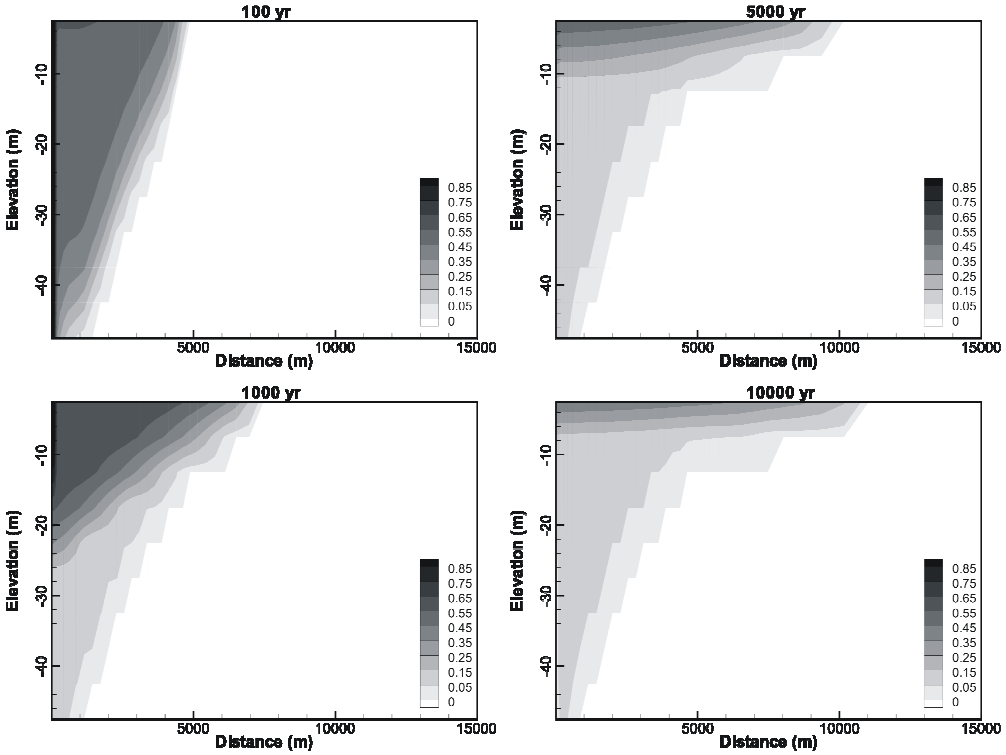
100 yr
5000 yr
1000 yr
10000 yr
Elevation (m)
-10
-20
-30
-40
5000
10000
15000
Distance (m)
0.85
0.75
0.65
0.55
0.45
0.35
0.25
0.15
0.05
0

Fig. 6

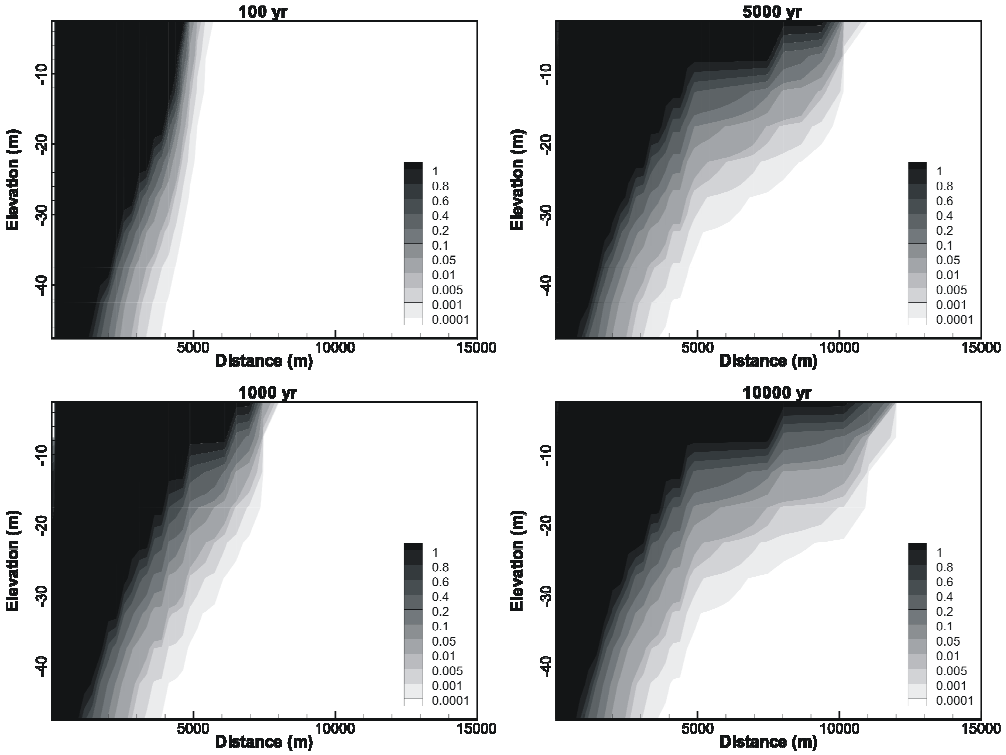
100 yr
5000 yr
1000 yr
10000 yr
Elevation (m)
-10
-20
-30
-40
5000
10000
15000
Distance (m)
1
0.8
0.6
0.4
0.2
0.1
0.05
0.01
0.005
0.001
0.0001

Fig. 7

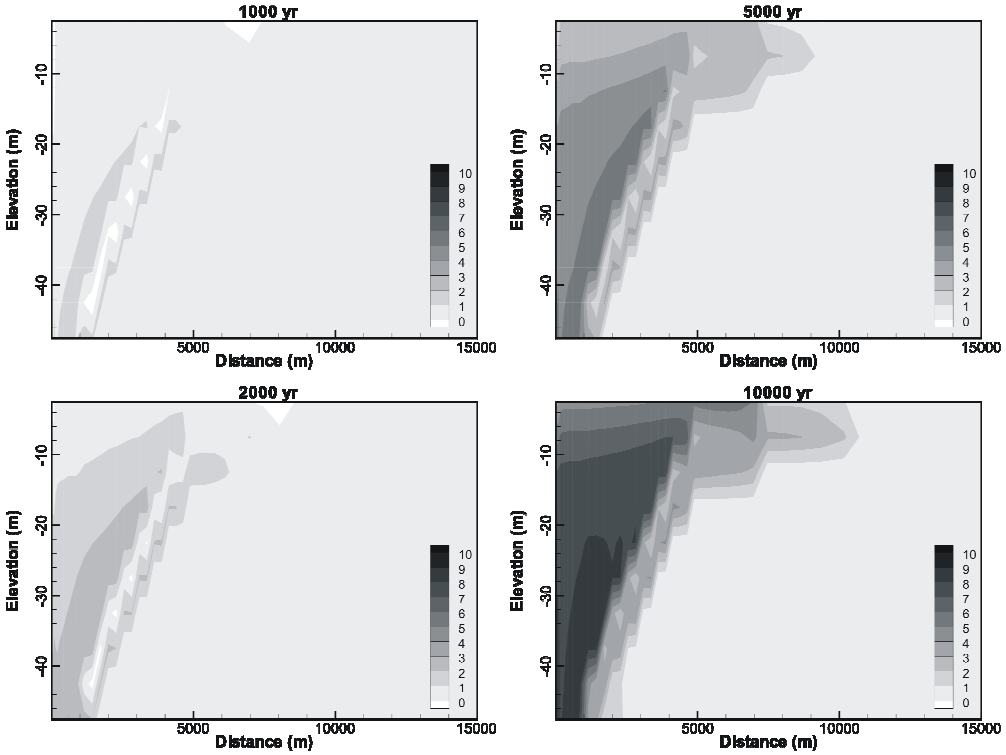
1000 yr
5000 yr
2000 yr
10000 yr
Elevation (m)
-10
-20
-30
-40
5000
10000
15000
Distance (m)
10
9
8
7
6
5
4
3
2
1
0

Fig. 8

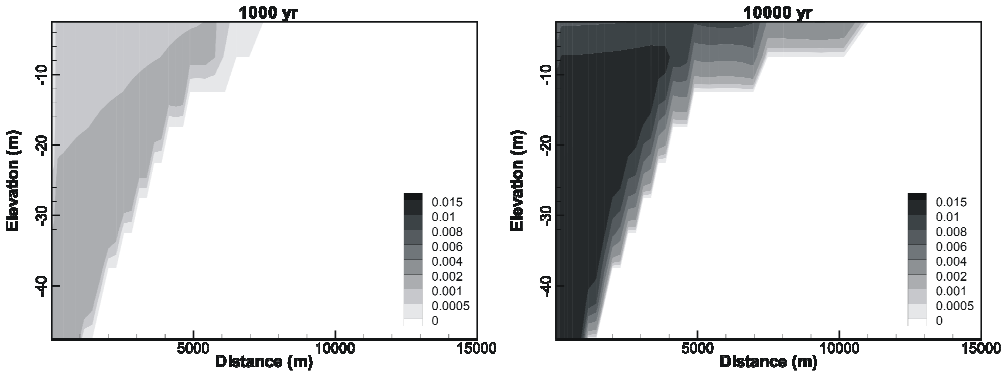
1000 yr
10000 yr
Elevation (m)
-10
-20
-30
-40
0.015
0.01
0.008
0.006
0.004
0.002
0.001
0.0005
0
5000
10000
15000
Distance (m)

Fig. 9

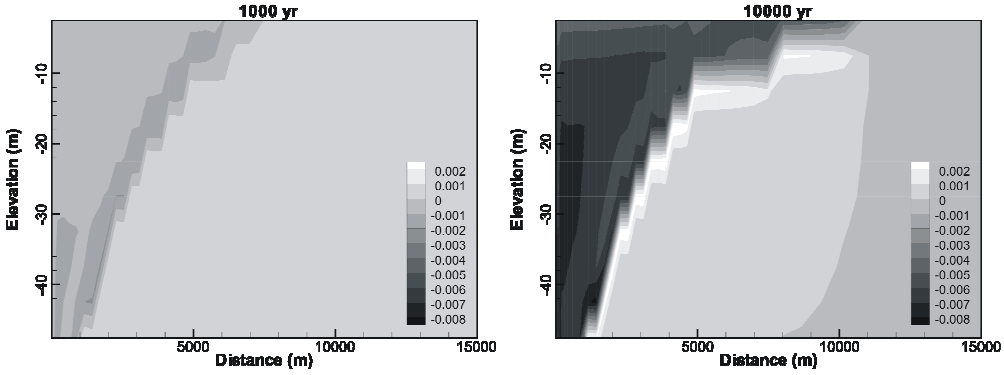
1000 yr
10000 yr
Elevation (m)
-10
-20
-30
-40
0.002
0.001
0
-0.001
-0.002
-0.003
-0.004
-0.005
-0.006
-0.007
-0.008
5000
10000
15000
Distance (m)

Fig. 10

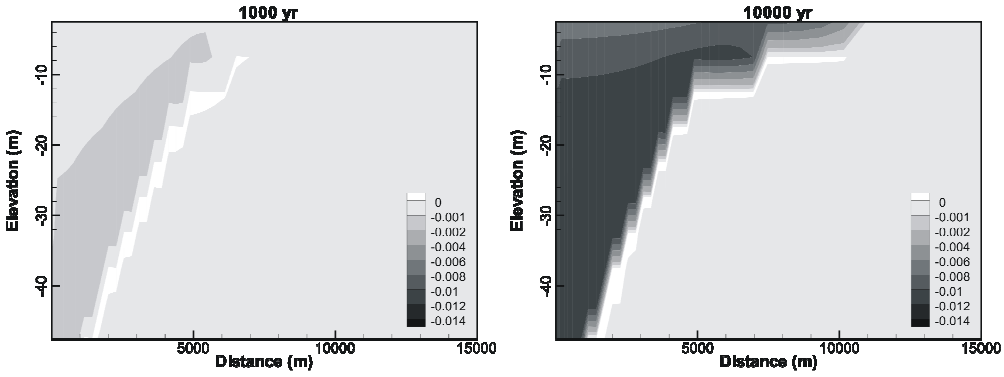
1000 yr
10000 yr
Elevation (m)
-10
-20
-30
-40
5000
10000
15000
Distance (m)
0
-0.001
-0.002
-0.004
-0.006
-0.008
-0.01
-0.012
-0.014

Fig. 11

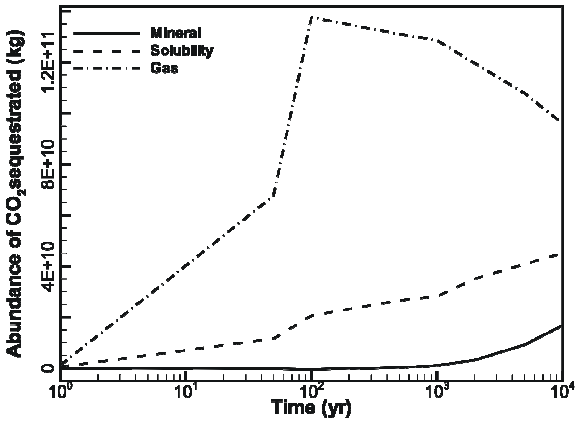
Mineral
Solubility
Gas
Abundance of CO2 sequestrated (kg)
0
4E+10
8E+10
1.2E+11
10^0
10^1
10^2
10^3
10^4
Time (yr)

Fig. 12

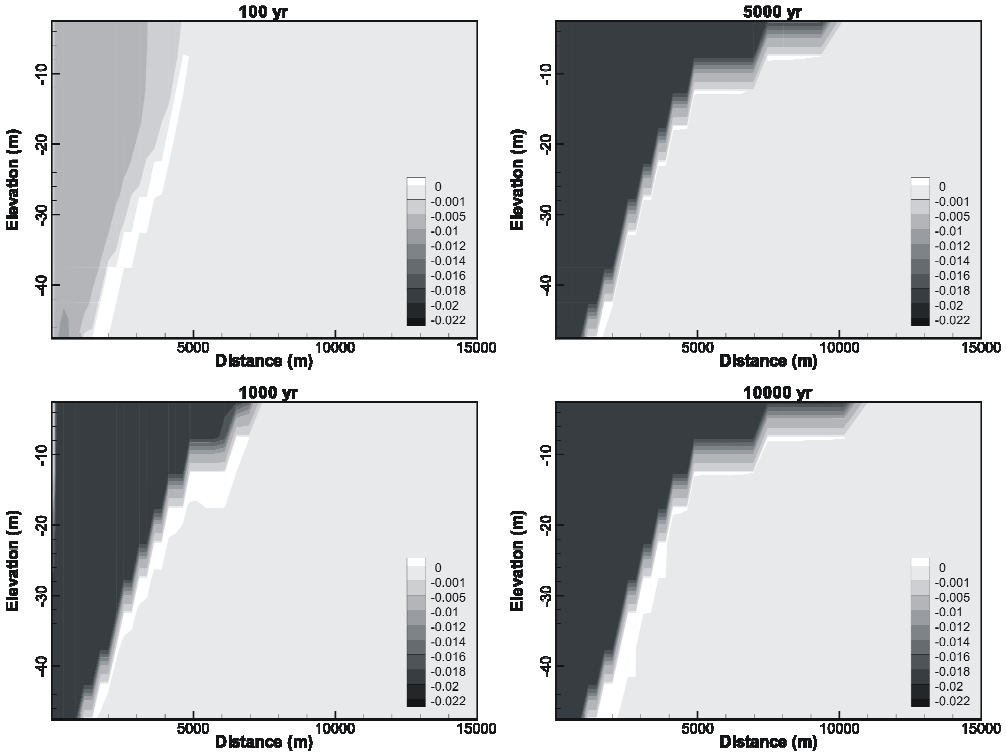
100 yr
5000 yr
1000 yr
10000 yr
Elevation (m)
-10
-20
-30
-40
5000
10000
15000
Distance (m)
0
-0.001
-0.005
-0.01
-0.012
-0.014
-0.016
-0.018
-0.02
-0.022

Fig. 13

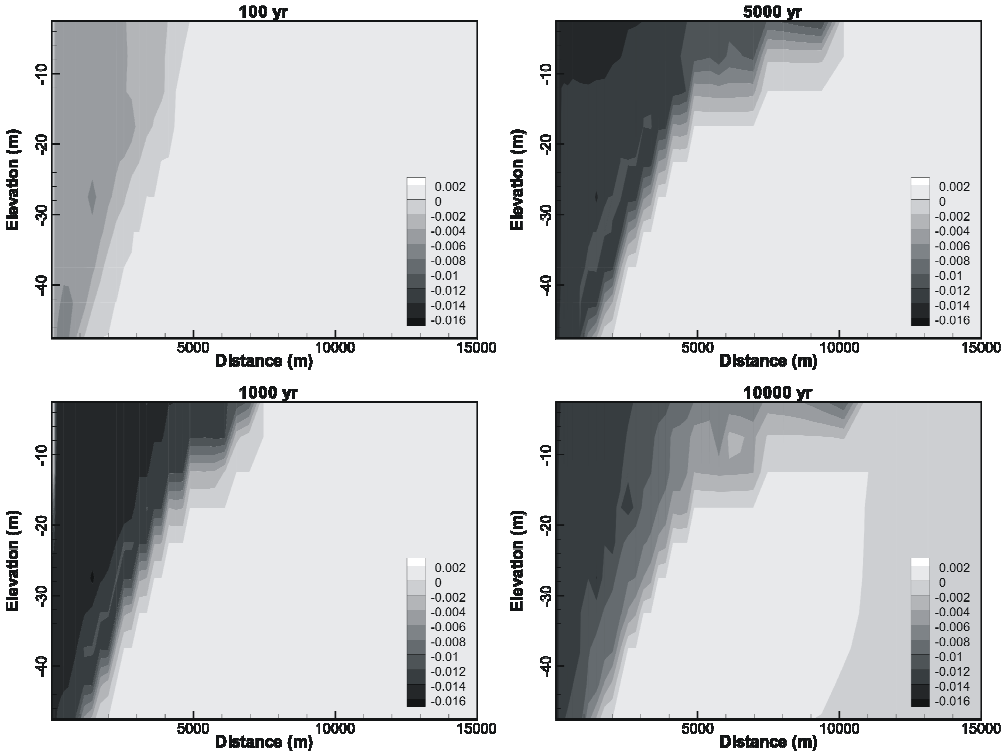
100 yr
5000 yr
1000 yr
10000 yr
Elevation (m)
-10
-20
-30
-40
5000
10000
15000
Distance (m)
0.002
0
-0.002
-0.004
-0.006
-0.008
-0.01
-0.012
-0.014
-0.016

Fig. 14

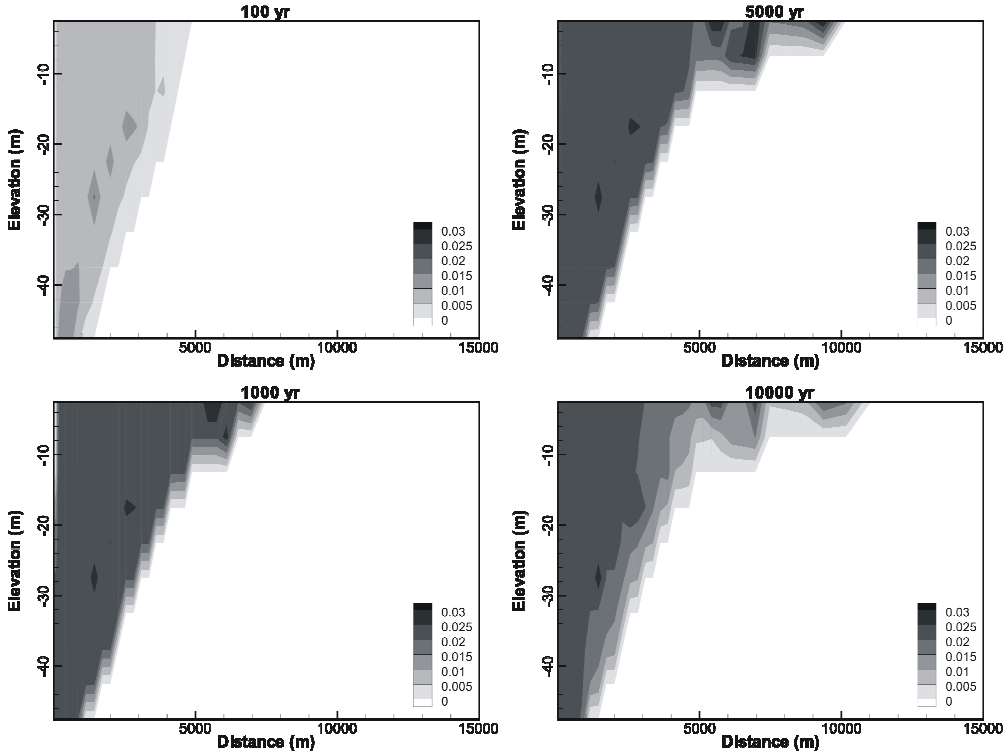
100 yr
5000 yr
1000 yr
10000 yr
Elevation (m)
-10
-20
-30
-40
5000
10000
15000
Distance (m)
0.03
0.025
0.02
0.015
0.01
0.005
0

Fig. 15

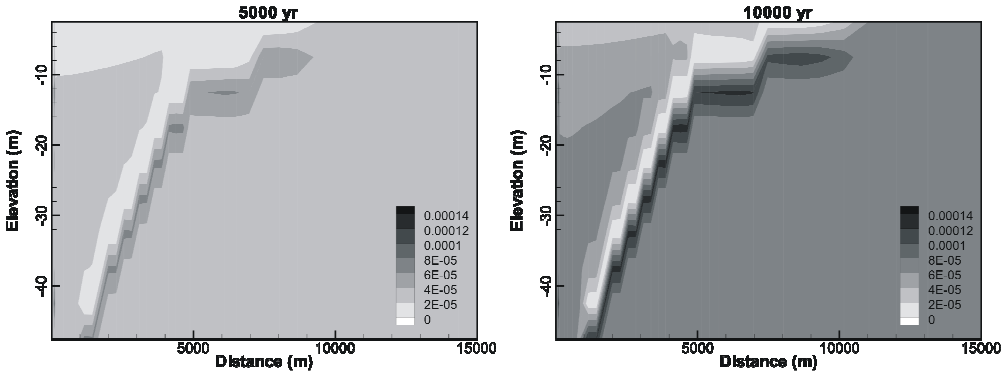
5000 yr
10000 yr
Elevation (m)
-10
-20
-30
-40
5000
10000
15000
Distance (m)
0.00014
0.00012
0.0001
8E-05
6E-05
4E-05
2E-05
0

Fig. 16

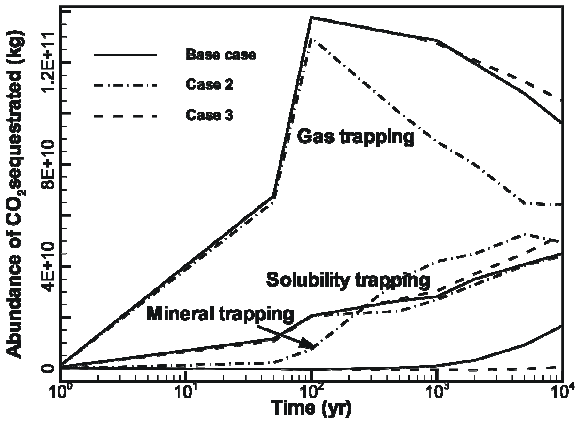
Abundance of CO2 sequestrated (kg)
0
4E+10
8E+10
1.2E+11
Base case
Case 2
Case 3
Gas trapping
Solubility trapping
Mineral trapping
10^0
10^1
10^2
10^3
10^4
Time (yr)

Fig. 17

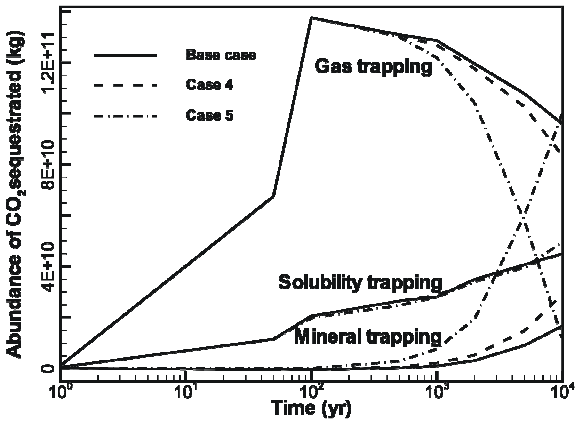
Base case
Case 4
Case 5
Gas trapping
Solubility trapping
Mineral trapping
Abundance of CO2 sequestrated (kg)
0
4E+10
8E+10
1.2E+11
10^0
10^1
10^2
10^3
10^4
Time (yr)

Fig. 18

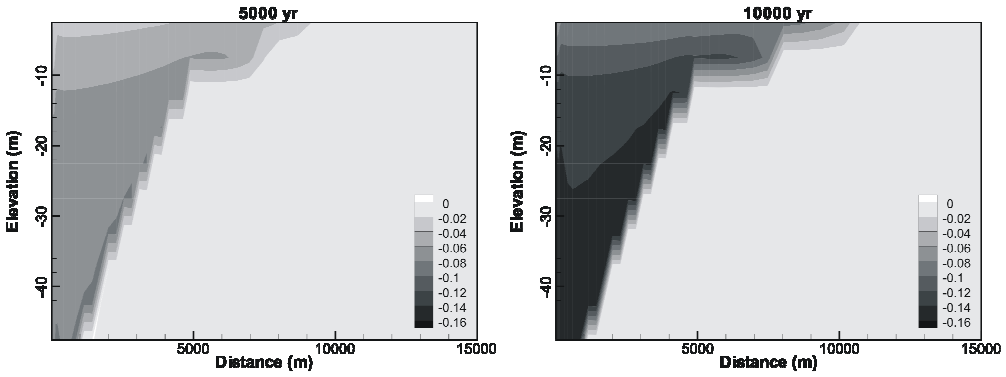
5000 yr
10000 yr
Elevation (m)
-10
-20
-30
-40
0
-0.02
-0.04
-0.06
-0.08
-0.1
-0.12
-0.14
-0.16
5000
10000
15000
Distance (m)

Fig. 19

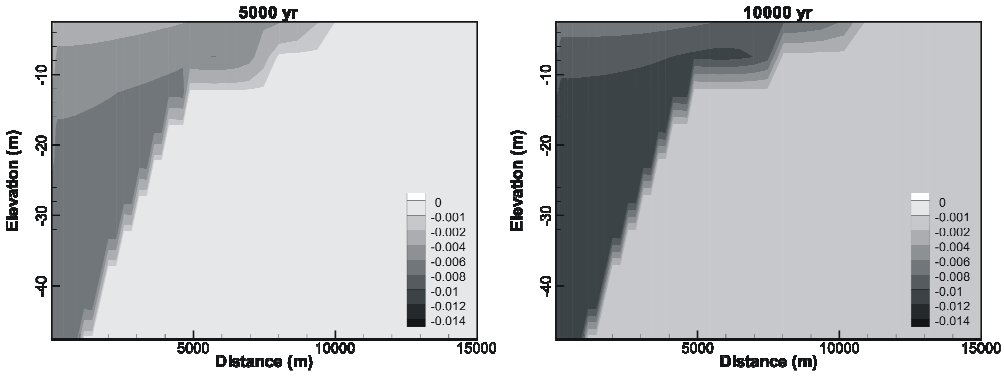
5000 yr
10000 yr
Elevation (m)
-10
-20
-30
-40
5000
10000
15000
Distance (m)
0
-0.001
-0.002
-0.004
-0.006
-0.008
-0.01
-0.012
-0.014

Fig. 20

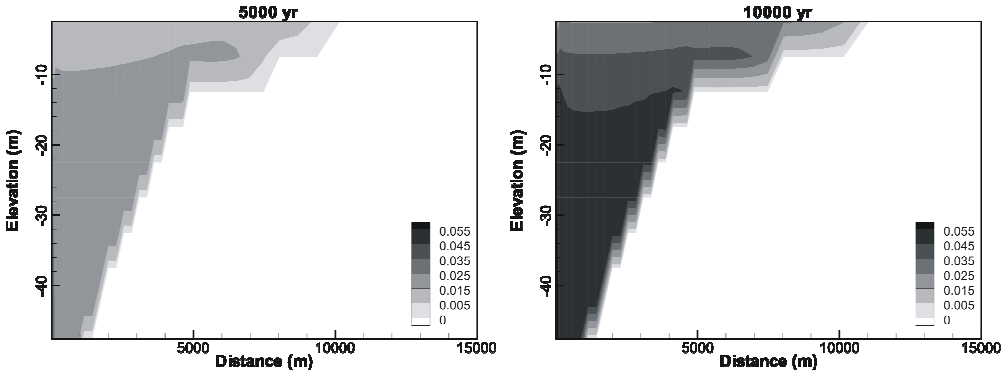
5000 yr
10000 yr
Elevation (m)
-10
-20
-30
-40
5000
10000
15000
Distance (m)
0.055
0.045
0.035
0.025
0.015
0.005
0

Fig. 21

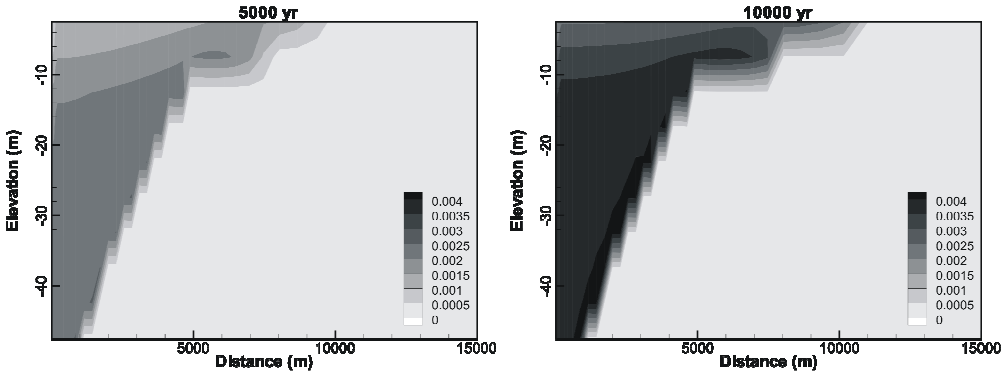
5000 yr
10000 yr
Elevation (m)
-10
-20
-30
-40
0.004
0.0035
0.003
0.0025
0.002
0.0015
0.001
0.0005
0
5000
10000
15000
Distance (m)

Fig. 22

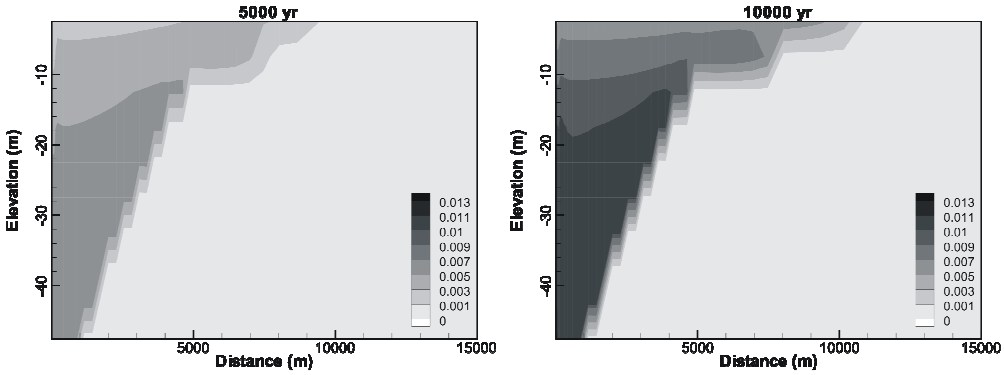
5000 yr
10000 yr
Elevation (m)
-10
-20
-30
-40
0.013
0.011
0.01
0.009
0.007
0.005
0.003
0.001
0
5000
10000
15000
Distance (m)

Fig. 23

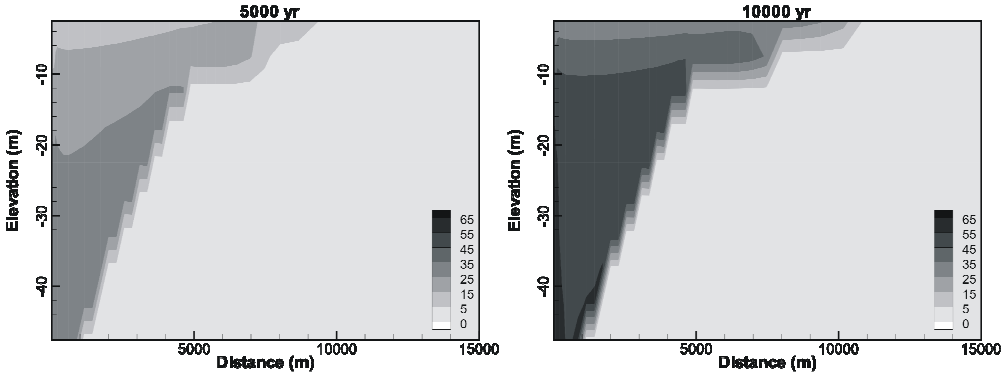
5000 yr
10000 yr
Elevation (m)
-10
-20
-30
-40
5000
10000
15000
Distance (m)
65
55
45
35
25
15
5
0

Fig. 24

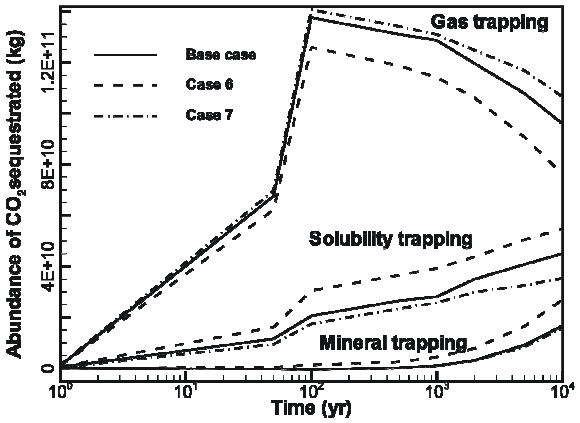
Gas trapping
Base case
Case 6
Case 7
Solubility trapping
Mineral trapping
Abundance of CO2 sequestrated (kg)
0
4E+10
8E+10
1.2E+11
10^0
10^1
10^2
10^3
10^4
Time (yr)

Fig. 25

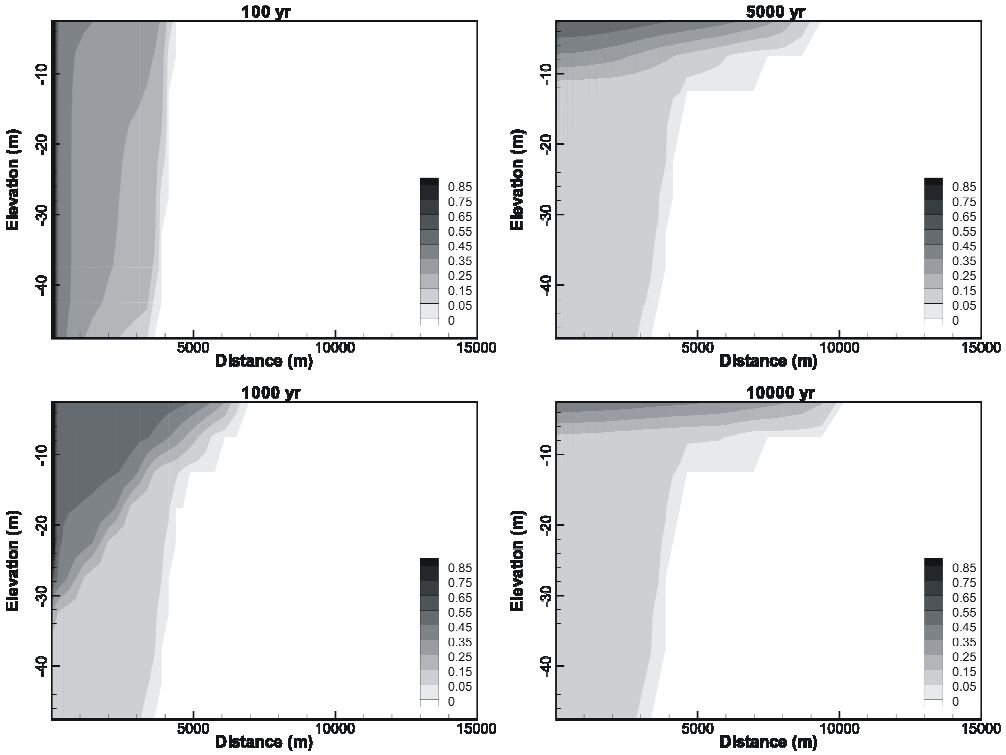
100 yr
5000 yr
1000 yr
10000 yr
Elevation (m)
-10
-20
-30
-40
5000
10000
15000
Distance (m)
0.85
0.75
0.65
0.55
0.45
0.35
0.25
0.15
0.05
0

Fig. 26

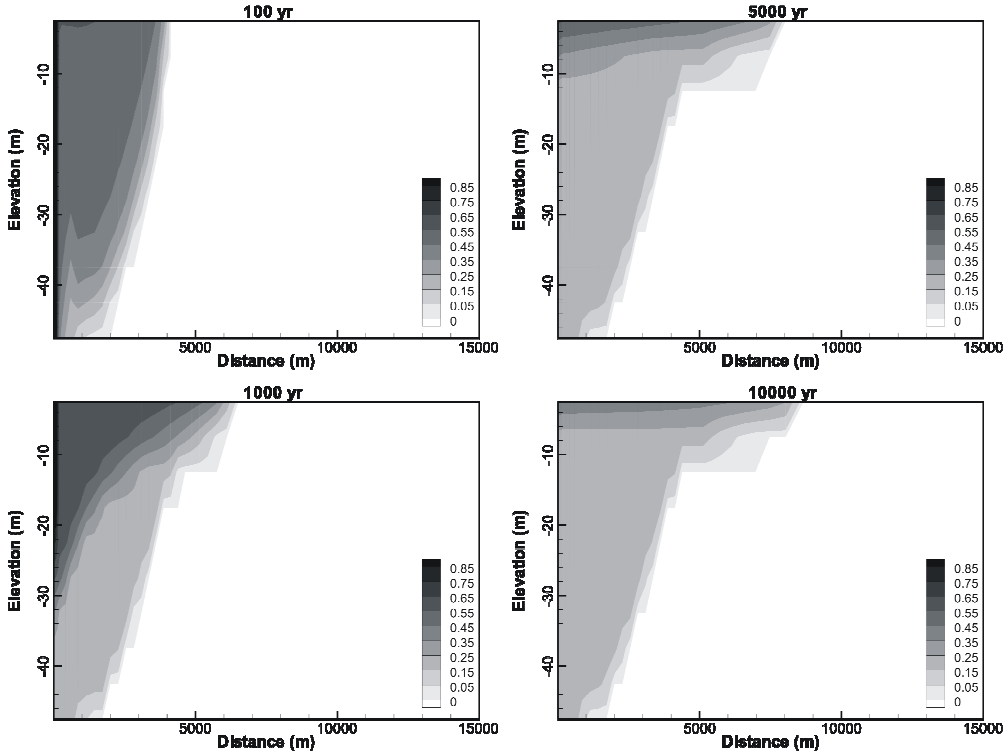
100 yr
5000 yr
1000 yr
10000 yr
Elevation (m)
-10
-20
-30
-40
5000
10000
15000
Distance (m)
0.85
0.75
0.65
0.55
0.45
0.35
0.25
0.15
0.05
0

Table 1.
Hydrogeological parameters used in the simulations.

Parameters	Sandstone formation
Porosity	0.30
Permeability (m^2)	1.0×10^{-13}
Ratio of vertical to horizontal permeability	0.5
Compressibility (Pa^{-1})	4.5×10^{-10}
Diffusivity (m^2/s)	1.0×10^{-9}
Rock grain density (kg/m^3)	2600
Formation heat conductivity (W/m ^oC)	2.51
Rock grain specific heat (J/kg ^oC)	920
Temperature (^oC)	50
Pressure (bar)	120
Relative permeability model:	
Liquid (Van Genuchten)	
$k_{rl} = \sqrt{S^*}\left\{1-(1-\left[S^*\right]^{1/m})^m\right\}^2$	$S^* = (S_l - S_{lr})/(1-S_{lr})$
S_{lr} : residual water saturation	S_{lr} = 0.30
m : exponent	m = 0.457
Gas (Corey):	
$k_{rg} = (1-\hat{S})^2(1-\hat{S}^2)$	$\hat{S} = (S_l - S_{lr})/(S_l - S_{lr} - S_{gr})$
S_{gr} : residual gas saturation	S_{gr} = 0.05
Capillary pressure model (Van Genuchten):	
$P_{cap} = -P_0(\left[S^*\right]^{-1/m} - 1)^{1-m}$	$S^* = (S_l - S_{lr})/(1-S_{lr})$
S_{lr} : residual water saturation	S_{lr} = 0.00
m : exponent	m = 0.457
P_0 : strength coefficient	P_0 = 19.61 kPa

Table 2.
Mineralogical composition of the Songliao Basin derived from the lithology slice analysis of clastic rocks, initial mineral volume fractions introduced in the model, and possible secondary mineral phases used in the simulations.

Sandstone mineral compositions	Volume fraction	Minerals used in the model	Chemical composition	Volume fraction used in the model
		Primary minerals		
Quartz	0.2570	Chalcedony	SiO_2	0.258
Kaolinite	0.0087	Kaolinite	$Al_2Si_2O_5(OH)$	0.009
Illite	0.0275	Illite	$K_{0.6}Mg_{0.25}Al_{1.8}(Al_{0.5}Si_{3.5}O_{10})(OH)_2$	0.028
Chlorite	0.0268	Chlorite	$Mg_{2.5}Fe_{2.5}Al_2Si_3O_{10}(OH)_8$	0.027
Calcite	0.0303	Calcite	$CaCO_3$	0.030
Plagioclase	0.4148	Albite~low	$NaAlSi_3O_8$	0.415[1]/0[2]
		Oligoclase	$Ca_{0.2}Na_{0.8}Al_{1.2}Si_{2.8}O_8$	0[1]/0.415[2]
K-feldspar	0.2328	K-feldspar	$KAlSi_3O_8$	0.233
Zeolite	0.0010	Not used		--
Pyrite	0.0004	Not used		--
Anhydrite	0.0007	Not used		--
		Total		1.0
		Secondary minerals		
		Magnesite	$MgCO_3$	0
		Dolomite	$CaMg(CO_3)_2$	0
		Siderite	$FeCO_3$	0
		Dawsonite	$NaAlCO_3(OH)_2$	0
		Ankerite	$CaMg_{0.3}Fe_{0.7}(CO_3)_2$	0
		Na-smectite	$Na_{0.290}Mg_{0.26}Al_{1.77}Si_{3.97}O_{10}(OH)_2$	0
		Ca-smectite	$Ca_{0.145}Mg_{0.26}Al_{1.77}Si_{3.97}O_{10}(OH)_2$	0

[1] Plagioclase composition for case 1 (base case).
[2] Plagioclase composition for case 5.

Table 3. Initial concentrations of the formation water at reservoir conditions of 50°C and 120 bars. (Iron is the sum of Fe^{2+}, Fe^{3+} and their related complexes. Carbon is the sum of CO_2(aq), CH_4(aq), and their related species such as HCO_3^- and acetic acid(aq). Sulfur is the sum of sulfate and sulfide species. Redox reactions are set using O_2(aq))

Parameter	Value	Elements	Concentration (mol/kg H_2O)
Temperature (°C)	50	Al	0.1362×10^{-07}
pH	8.348	Carbon	0.3717×10^{-01}
		Ca	0.3233×10^{-04}
		Cl	$0.1697\times10^{+00}$
		Iron	0.4100×10^{-06}
		K	0.9366×10^{-03}
		Mg	0.3819×10^{-07}
		Na	$0.2354\times10^{+00}$
		Sulfur	0.1000×10^{-19}
		Si	0.6167×10^{-03}
		O_2(aq)	0.177×10^{-66}

Table 4.

List of parameters for calculating kinetic rate constants of minerals. Note that: (1) all rate constants are listed for dissolution; (2) k_{25} is kinetic constant at 25°C, E_a is activation energy, and n is the power term (Eq. 2); (3) the power terms n for both acid and base mechanisms are with respect to H^+.

Minerals	Surface area (cm^2/g)	Parameters for kinetic rate law							
		Neutral mechanism		Acid mechanism			Base mechanism		
		k_{25} (mol/m^2 s)	E_a (kJ/mol)	k_{25}	E_a	$n\ (H^+)$	k_{25}	E_a	$n\ (H^+)$
Calcite	--	Equilibrium	--						
Chalcedony	9.8	1.2500e-14	87.5						
Kaolinite	151.6	6.9183e-14	22.2	4.8978e-12	65.9	0.777	8.9125e-18	17.9	-0.472
Illite	151.6	1.6596e-13	35.0	1.0471e-11	23.6	0.34	3.0200e-17	58.9	-0.40
Chlorite	9.8	3.0200e-13	88.0	7.7624e-12	88.0	0.5			
Albite~low	9.8	2.7542e-13	69.8	6.9183e-11	65.0	0.457	2.5119e-16	71.0	-0.572
Oligoclase	9.8	1.4451e-12	69.8	2.1380e-10	65.0	0.457			
K-feldspar	9.8	3.8905e-13	38.0	8.7096e-11	51.7	0.5	6.3096e-22	94.1	-0.823
Magnesite	9.8	4.5709e-10	23.5	4.1687e-07	14.4	1.0			
Dolomite (sedimentary disordered)	9.8	2.9512e-08	52.2	6.4565e-04	36.1	0.5			
Siderite	9.8	1.2598e-09	62.76	6.4565e-04	36.1	0.5			
Dawsonite	9.8	1.2598e-09	62.76	6.4565e-04	36.1	0.5			
Ankerite	9.8	1.2598e-09	62.76	6.4565e-04	36.1	0.5			
Na-smectite	151.6	1.6596e-13	35.0	1.0471e-11	23.6	0.34	3.0200e-17	58.9	-0.40
Ca-smectite	151.6	1.6596e-13	35.0	1.0471e-11	23.6	0.34	3.0200e-17	58.9	-0.40